NeuroImage: Clinical 44 (2024) 103687

Contents lists available at ScienceDirect

NeuroImage: Clinical

journal homepage: www.elsevier.com/locate/ynicl

# Hypothalamic atrophy and structural covariance in amnestic mild cognitive impairment and Alzheimer's dementia

Hannah Pecher [a,b,*], Melanie Storch [c,d], Frauke Beyer [e], Veronica Witte [e], Christian-Frank Baasner [a], Peter Schönknecht [f,g,h], Christopher M. Weise [a], for the Alzheimer's Disease Neuroimaging Initiative [1]

[a] Department of Neurology, Martin-Luther-University Halle-Wittenberg, 06120 Halle (Saale), German
[b] Department of Radiology, Bundeswehrkrankenhaus Berlin, Scharnhorststr. 13, 10115 Berlin, Germany
[c] Department of Psychiatry and Psychotherapy, University Hospital Leipzig, Semmelweisstr. 10, 04103 Leipzig, Germany
[d] Department of Biology, University of Leipzig, 04103 Leipzig, Germany
[e] Department of Neurology, Max Planck-Institute for Human Cognitive and Brain Sciences, and Cognitive Neurology, University of Leipzig Medical Center, Leipzig, Germany
[f] Medical Faculty, Department of Psychiatry and Psychotherapy, University Hospital Leipzig, 04103 Leipzig, Germany
[g] Out-Patient Department for Sexual-Therapeutic Prevention and Forensic Psychiatry, University Hospital Leipzig, 04103, Leipzig, Germany
[h] Academic Saxon State Hospital Altscherbitz, 04435 Schkeuditz, Germany

ARTICLE INFO

*Keywords:*
Hypothalamic atrophy
Alzheimer's disease
Volumetry
Structural covariance networks
Mild cognitive impairment

ABSTRACT

*Background:* Alzheimer's disease (AD) is characterized by progressive cognitive decline and specific brain atrophy patterns, primarily involving the medial temporal lobes. A number of studies have discussed hypothalamic involvement in AD with consecutive metabolic and/or autonomic disturbances yet only few studies have investigated hypothalamic atrophy in AD and its early stages in particular. *Methods:* We applied semi-automated volumetry of the hypothalamus (HTH) in 3 T MRI in a sample N = 175 participants [age 74.9 ± 7.22; gender 85 m/90f; cognitively normal controls (CN; N = 56); amnestic mild cognitive impairment (MCI; N = 78); AD (N = 41)] from the Alzheimer's Disease Neuroimaging Initiative (ADNI). In addition, we used voxel-based morphometry (VBM), cortical thickness (CTH) analyses and source-based morphometry (SBM) derived networks of structural covariance to investigate brain structural covariance patterns of the HTH under consideration of diagnostic groups, β-amyloid (AB) positivity and apolipoprotein E (APOE) ε4 status. *Results:* Hypothalamic atrophy was observed in both early and advanced disease stages (i.e. hypothalamic volume CN > MCI > AD). VBM, CTH analysis and SBM revealed positive associations between hypothalamic volume (HV) and AD-vulnerable regions, largely corresponding to the Papez circuit and brain regions implicated in autonomic regulation, however, group differences regarding HTH structural covariance were not observed. Similar observations were made in carriers and non-carriers of the ε4 allele, yet more pronounced in ε4 carriers. Although not reaching significance, comparisons of AB positive vs. negative subjects indicated stronger HTH atrophy in biomarker positive participants. HV was not associated with body mass index or longitudinal weight change. *Conclusions*: Our findings support early structural changes of the HTH in AD. HV covaries with regional volumes of AD-vulnerable regions. This could point to secondary atrophy of the HTH following atrophy of the hippocampus and other structures of the Papez circuit in AD.

* Corresponding author at: Hannah Pecher, Department of Radiology, Bundeswehrkrankenhaus Berlin, Scharnhorststr. 13, 10115 Berlin, Germany.
*E-mail address:* HannahPecher@bundeswehr.org (H. Pecher).

[1] Data used in preparation of this article were obtained from the Alzheimer's Disease Neuroimaging Initiative (ADNI) database (adni.loni.usc.edu). As such, the investigators within the ADNI contributed to the design and implementation of ADNI and/or provided data but did not participate in analysis or writing of this report. A complete listing of ADNI investigators can be found at: http://adni.loni.usc.edu/wp-content/uploads/how_to_apply/ADNI_Acknowledgement_List.pdf.

https://doi.org/10.1016/j.nicl.2024.103687
Received 5 May 2024; Received in revised form 10 September 2024; Accepted 8 October 2024
Available online 11 October 2024

## 1. Introduction

Alzheimer's dementia (AD) is the most common neurodegenerative dementia with high socioeconomic relevance (Reitz et al. 2011; Prince et al. 2013; Nichols et al. 2019). The characteristic neuropathological correlate for AD pathogenesis is the formation of extracellular β-Amyloid (AB) plaques and intracellular aggregates of hyperphosphorylated tau protein, which are understood to propagate throughout the brain in a characteristic pattern over the course of the disease (Braak and Braak 1991; Walker 2018). Although many genetic and acquired risk factors have been identified there still remains uncertainty regarding the underlying causes of AD development and progression (Edwards et al., 2019); Silva et al. 2019).

Recent studies have linked pathological and clinical changes in AD to the hypothalamus (HTH), a small but densely interconnected diencephalic brain region with a variety of functions and regulatory tasks (Ishii and Iadecola 2015). For instance, the HTH is a key regulatory centre for the autonomic nervous system (Ulrich-Lai and Herman 2009), strongly connected to AD-typical structures like the hippocampus via the fornix (Papez 1937; Choi et al. 2019). Thus, hypothalamic dysfunction could influence metabolic and non-cognitive changes in AD, causing early symptoms like late-life weight loss and circadian disruption, although the full extent to which the HTH is affected in AD remains unclear (Hiller and Ishii 2018). As an indicator of hypothalamic involvement in AD, neuropathological studies have found AB plaques and neurodegeneration in hypothalamic nuclei of AD patients (Ogomori et al. 1989; Baloyannis et al. 2015). Brain atrophy – particularly atrophy of the medial temporal lobe and the hippocampus – has been well-established as an imaging biomarker in AD (Scheltens et al. 2016; Jack et al. 2013; Colliot et al. 2008; Whitwell et al. 2011), however, volumetric studies also suggest that AD might be associated with hypothalamic atrophy even early in the disease course (Baron et al. 2001; Copenhaver et al. 2006; Hall et al. 2008).

As the HTH is part of a large neural network (Kim et al. 2022), we hypothesized that hypothalamic atrophy could have implications on other structures as well. Conversely, degeneration and atrophy in other brain regions in AD could lead to secondary changes in the HTH. Thus far, few studies have investigated hypothalamic involvement in AD, mostly using common neuroimaging methods such as voxel-based morphometry (VBM; (Ashburner and Friston 2000)). However, methods such as VBM have limitations with respect to small subcortical regions such as the HTH, e.g. (Senjem et al. 2005; Wonderlick et al. 2009; Zhou et al. 2022; Ashburner and Friston 2000), therefore we chose to re-evaluate involvement of the HTH in AD via a semi-automated algorithm that had been specifically developed for hypothalamic volumetry (Wolff et al. 2018). In addition, we aimed to explore the relationship of hypothalamic volume (HV) with clinical parameters and genetic risk factors (i.e. ApoE status) as well as its structural covariance by making use of VBM, cortical thickness analysis (CTH) and source-based morphometry (SBM) derived structural covariance networks.

## 2. Methods

For an overview of our workflow see Fig. 1.

### 2.1. Study population

Data used for this study was downloaded from the Alzheimer's Disease Neuroimaging Initiative (ADNI) database (https://adni.loni.usc.edu/). Diagnosis of amnestic MCI and AD was standardised according to the Petersen criteria (Petersen et al. 2010); using the Mini-Mental-State Examination (MMSE; (Folstein et al. 1975)), Clinical Dementia Rating scale (CDR, (Hughes et al. 1982)) and the Logical Memory II subscale of the Wechsler Memory Scale-Revised (Sullivan 2005) for cognitive testing. In ADNI 1, structural images were obtained using 1.5 T- and 3 T-scanners with the following parameters: 8-channel coil, TR = 650 ms, TE = min full, flip-angle = 8°, slice thickness = 1.2 mm, resolution = 256 × 256 mm and FOV = 26 cm. ADNI pre-processing of MPRAGE images in ADNI 1 included gradwarp correction of distortions caused by non-linear gradients, B1 non-uniformity correction and N3 processing for each MPRAGE image (https://adni.loni.usc.edu/methods/mri-tool/mri-pre-processing/). For a detailed description of

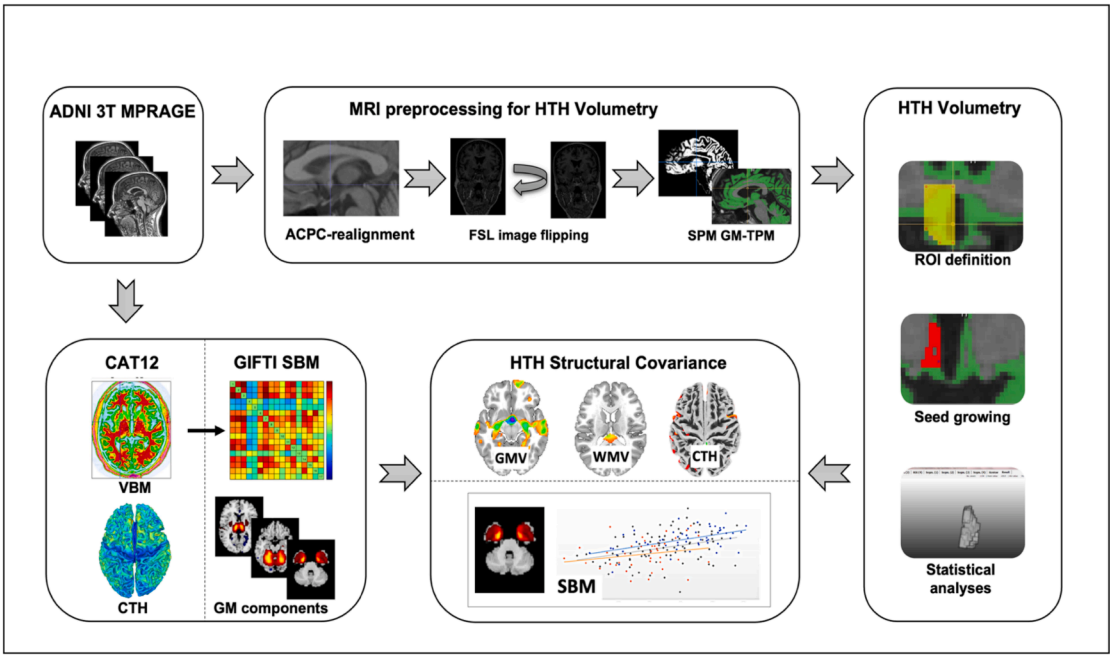


**Fig. 1.** Illustrated workflow showing processing of ADNI 3 T MPRAGE data for hypothalamic volumetry as well as structural covariance analysis with SPM12 software and the CAT12 toolbox implemented in SPM12. *ADNI* Alzheimer's disease neuroimaging initiative, *ACPC* anterior commissure posterior commissure, *CAT12* computational anatomy toolbox, *CTH* cortical thickness, *GM-TPM* gray matter tissue probability map, *GMV* gray matter volume, *HTH* hypothalamus, *ROI* region of interest, *SBM* source-based morphometry, *SPM* statistical parametric mapping, *VBM* voxel-based morphometry, *WMV* white matter volume.

structural imaging protocols as well as information on the acquisition and processing of imaging data as well as biological markers please refer to the ADNI website (https://adni.loni.usc.edu/methods/). Following ADNI recommendations, we made use of a standardized 3 T subsample from the ADNI 1 cohort (Wyman et al. 2013). Furthermore, we included 25 additional subjects with structural 3 T MPRAGE data with identical pre-processing and sufficient quality. In total, our sample comprised n = 176 subjects, one of which was later excluded due to substantial artifacts. Thus, we included a total of n = 175 subjects, n = 78 subjects with amnestic mild cognitive impairment (MCI), n = 41 subjects with AD and n = 56 cognitively normal (CN) controls. CSF AD biomarkers (i.e. "UPENNBIOMK_MASTER_FINAL" dataset) were available for N = 95. Here, AB positivity was defined by AB 1–42 < 192 pg/mL, as previously established (Shaw et al. 2009).

### 2.2. MR image pre-processing for hypothalamic volumetry

Hypothalamic volumetry was performed with a semi-automated approach according to the protocol by Wolff et al. (2018). Data were first carefully checked for relevant artifacts and then realigned to position the centres of the anterior and posterior commissure on the same horizontal level (i.e. "ACPC" orientation). Realignment was done using ITK-SNAP. Next, image flipping was performed using FSL software (https://fsl.fmrib.ox.ac.uk/fsl/fslwiki/FSL). After flipping, both the right and the left hypothalamus were displayed on the same half of the screen, thus allowing the rater to always apply the algorithm in the same way irrespective of hemisphere. We then calculated gray matter tissue probability maps (GM-TPM) which would later serve as an overlay over the anatomical T1-weighted image, using Statistical Parametric Mapping software (SPM12, Wellcome Department of Imaging Neuroscience, London, UK; https://www.fil.ion.ucl.ac.uk/spm/) in MATLAB.

### 2.3. Semi-automated volumetry of the hypothalamus

Hypothalamic volumetry was performed with MeVisLab 3.4.1 (https://www.mevislab.de/) using the algorithm for semi-automated volumetry published by Wolff et al. (2018): In brief, the rater manually defines four regions of interest (ROIs) using anatomical landmarks in the T1-weighted image as well as the GM-TPM-overlay as reference. ROI 1 corresponds to the preoptic HTH situated in the same coronal plane as the anterior commissure. Caudal of ROI 1, the intermediate superior (ROI 2) and intermediate inferior (ROI 3) HTH begins with the opening of the interventricular foramen in coronal view. Special emphasis is put on including all lateral hypothalamic voxels yet excluding the fornix and the optic tract. Finally, ROI 4 encompasses the mamillary bodies. A detailed summary and visualisation of the algorithm landmarks is provided in the original article by Wolff et al. (2018). In the next step, the rater chooses one voxel within the HTH as a starting point for volumetric segmentation by seed-growing technology. The software then includes all voxels within the ROIs if they are within predefined thresholds to calculate HV. In a third step the rater reviews and adjusts the segmentation result in triplanar view. The left and right HTH were segmented separately with this method. The rater was blinded for the whole process. Before volumetric assessment of our sample, we adapted the lower GM-TPM thresholds to our dataset as trial runs showed that hypothalamic voxels, especially in the preoptic ROI, were falsely excluded in our segmentation results (new lower thresholds: ROI 1: *0.47*; ROI 2: *0.3*; ROI 3: *0.33*; ROI 4: *0.22*; original thresholds according to Wolff et al. (2018): ROI 1: 0.65; ROI 2: 0.05; ROI 3: 0.05; ROI 4: 0.01). When adapting the thresholds we were also careful to prevent inclusion of non-hypothalamic voxels in the intra- and periventricular areas as faulty voxel inclusion in these areas has been previously described (Thomas et al. 2019). Wolff et al. (2018) reported good interrater reliabilities in their methodological paper (ICC 0.78 to 0.82)) with voxel-wise overlap of appr. 90. To additionally determine intrarater reliability in our study, the rater segmented the hypothalami of a representative sample of N = 40 subjects twice, again blinded and after additional pseudonymization of image descriptions. Intrarater reliability was found to be excellent with an intraclass correlation coefficient (ICC) of 0.978. Finally, semi-automated volumetry was performed on N = 175 subjects and total HV was calculated as a sum of left and right HV.

### 2.4. MR image preprocessing for VBM and CTH analysis

We conducted VBM (Ashburner and Friston 2000) and CTH analysis of 3D MPRAGE data with SPM12 and the Computational Anatomy Toolbox 12 (CAT12; https://dbm.neuro.uni-jena.de/cat.html) within the MATLAB (https://www.mathworks.com) framework. Preprocessing for VBM analyses was performed with default settings of the CAT12 toolbox, which include corrections for bias-field inhomogeneities, segmentation into gray matter (GM), white matter (WM), and cerebrospinal fluid (CSF), followed by spatial normalization to the DARTEL template in MNI space (voxel size: 1.5 mm x 1.5 mm x 1.5 mm). After preprocessing we performed smoothing with an 8 mm full-width-half-maximum (FWHM) isotropic Gaussian kernel (VBM data). For surface-based analyses of CTH, cortical thickness was estimated with the projection-based thickness method (Dahnke et al. 2013) while also receiving estimations of the central surface of both hemispheres, as implemented in the CAT12 toolbox. CTH data were smoothed with a 15 mm FWHM kernel.

### 2.5. Statistical analysis

Statistical analysis of non-imaging data, volumetric data of the hypothalamus and source based morphometry (SBM) derived data was performed using SAS statistical software (SAS Institute Inc, version 9.4, Cary, NC). Statistical neuroimaging analyses were done with SPM12 and CAT12 within the MATLAB framework. Violin plots were created using GraphPad Prism version 10.0.0 for Windows, GraphPad Software, Boston, Massachusetts USA, www.graphpad.com.

#### 2.5.1. Hypothalamic volume (HV)

One-way analysis of variance (ANOVA) followed by post-hoc Duncan's multiple range test was used to test for group differences of right, left and total HV respectively. HV was residualized by correcting for age, gender, and total intracranial volume (TIV) within the general linear model (GLM). The resulting residual HV was used for further statistical analyses. We furthermore investigated the potential influence of APOE, AB positivity as well as the relationship of HV with body mass index (BMI) and 2-year weight loss using Spearman's partial correlation analysis.

#### 2.5.2. Voxel-based morphometry (VBM) and cortical thickness (CTH)

Structural covariance analyses (Mechelli et al. 2005; Evans 2013) were performed to investigate potential group differences regarding the relationship of HV with gray matter volume (GMV) and CTH. Within SPM12, ANOVA with a group*hypothalamic_volume interaction term was conducted using HV as seed and adjusting for age, gender and TIV (VBM only). Similar analyses were made for the interaction of carriers vs. non-carriers of the APOE ε4 allele with HV with additional adjustment for diagnostic groups. To account for multiple comparisons Family-wise error (FWE) was applied, and statistical significance was set at $p < 0.05$ FWE cluster level corrected with a cluster-forming threshold of $p < 0.001$. In addition, we performed structural covariance analyses of HV across the whole sample via multiple regression analyses with additional adjustment for diagnostic groups. Here a more stringent threshold was applied with $p < 0.05$ FWE voxel-level corrected and an extent threshold of $k = 10$. In contrast to FWE cluster-level statistics, voxel-level statistics do not take into account the cluster size (i.e. the number of neighbouring voxels or vertices) of the respective results, rather than performing a multiple comparisons correction for each voxel or vertex individually, thus providing a far more conservative statistical

approach. Since for structural covariance analyses without group comparisons highly significant results were to be expected, we chose the latter for these particular analyses.

For quality assurance we also investigated the group specific atrophy patterns via ANOVA (data not shown).

#### 2.5.3. Source-based morphometry (SBM)

For SBM analyses of structural covariance networks, smoothed GM data from the VBM preprocessing pipeline were used. SBM is a multivariate approach for analysis of GM covariation (i.e. structural covariance networks). Methodological aspects are described in detail in (Xu et al. 2009). In brief: first, the number of components to be extracted from GMV data of our preprocessed sample of N = 175 subjects were estimated via the minimum description length (MDL) principle. This step identified N = 17 components in total which were covariant brain regions (C1 – C17). Next, spatial independent component analysis (ICA) was performed with the Infomax algorithm using the "Group ICA for fMRI Toolbox" (GIFT toolbox; https://trendscenter.org/software/gift/). All GMV images were used to compute a source matrix and a mixing matrix. Resulting subject- and component-wise, z-transformed loading coefficients, reflective of the contribution of each individual covariance pattern to the GM data of each individual participant can then be statistically analyzed. Similar to the previously described approach we first investigated potential group differences regarding the relationship of HV with the SBM components (i.e. group*component interaction term within the GLM) next to Spearman partial correlation analyses of HV and SBM components with age, gender, group and TIV as additional covariates. Due to the comparably large number of components, accounting for multiple comparisons was necessary. To do so, we applied a false discovery rate of $p < 0.05$ FDR-corrected to account for multiple comparisons (https://www.sdmproject.com/utilities/?show = FDR). FDR was chosen for its greater probability to reject the null hypothesis (as compared to a Bonferroni correction).

## 3. Results

### 3.1. Comparisons of hypothalamic volumes

Subject characteristics are summarized in Table 1.

Graphical illustrations of HV group differences can be found in Fig. 2.

HV differed statistically significant for all three diagnostic groups with highest volumes in CN subjects and lowest volumes in subjects with AD (ANOVA $p < 0.0001$; post hoc Duncan's Test: CN > MCI > AD). Similarly, volumes of the right HTH (ANOVA $p < 0.0001$) and left HTH (ANOVA $p < 0.0001$) showed significant group differences (i.e. CN > MCI > AD). Effect sizes (via Cohen's *d*) were moderate to high (for CN vs. MCI: 0.58; for CN vs. AD: 1.12; for MCI vs. AD: 0.55).

Carriers of the ε4-allele showed highly significant group differences regarding the right (ANOVA $p = 0.0001$), left (ANOVA $p < 0.0001$) and total HV (ANOVA $p < 0.0001$). Similar to the diagnostic group comparisons, largest volumes were measured in CN, followed by MCI and AD. Here Duncan's test revealed significant group differences for CN > MCI as well as CN > AD but not for MCI > AD. In **non**-carriers of the ε4-allele we observed significant group differences for left HV (ANOVA $p < 0.01$) and total HV (ANOVA $p = 0.02$) while only a trend was observed for the right HTH (ANOVA $p = 0.06$) with Duncan's test showing higher volumes in CN vs. AD only. Left HV in turn differed significantly between CN vs. AD i.e. CN > AD) as well as MCI and AD (i.e. MCI > AD) but not in CN and MCI. Lastly, total HV was significantly different only between CN and AD subjects in APOE ε4-non-carriers (i.e. CN > AD).

Additional sub-sample analyses of β-amyloid positive (AB+ ) vs. negative (AB-) subjects yielded slightly smaller HV in AB+ vs. AB- subjects, yet these results were not significant (pooled sample, n = 95, corrected for diagnostic groups; ANOVA $p = 0.65$). Looking at AB- subjects (n = 34) ANOVA showed significant differences regarding diagnostic groups (ANOVA $p = 0.03$), yet Duncan's test was not significant. For AB+ subjects (n = 61) both ANOVA and post-hoc Duncan's test were not significant (ANOVA $p = 0.06$). However, for the comparison of AB+ MCI and AB+ AD vs. AB- CN, ANOVA was significant ($p = 0.003$) and showed smaller HV in AD as compared to CN and MCI. Similarly to the pooled analyses, HV decreased across disease stages (i.e. CN > MCI > AD) although comparisons of CN vs. MCI and MCI vs. AD did not reach significance in post hoc Duncan's test. HV did not correlate with AB, total tau (t-tau) or phosphorylated tau (p-tau).

No significant associations were found for HV with body weight (i.e. BMI) or longitudinal weight changes.

**Table 1**
Subject characteristics.

| Group | CN (N = 56) | MCI (N = 78) | AD (N = 41) | total (N = 175) | p-value |
|---|---|---|---|---|---|
| Age in years | 75.5 ± 4.8 | 74.7 ± 7.93 | 74.5 ± 8.46 | 74.9 ± 7.22 | n.s. |
| Gender | | | | | 0.003 |
| female (N) | 35 (62.5 %) | 29 (37.2 %) | 26 (63.4) | 90 (51.4 %) | |
| male (N) | 21 (37.5 %) | 49 (62.8 %) | 15 (36.6 %) | 85 (48.6 %) | |
| BMI in kg/m$^2$ | 26.6 ± 4.4 | 25.1 ± 3.0 | 24.5 ± 3.9 | 25.4 ± 3.8 | 0.01 |
| Weight in kg | 74.4 ± 13.78 | 74.5 ± 12.50 | 67.8 ± 14.81 | 72.8 ± 13.8 | 0.02 |
| MMSE | 29.2 ± 0.8 | 25.7 ± 2.6 | 21.4 ± 3.5 | 25.8 ± 3.8 | 0<.0001 |
| CDR | 0 ± 0 | 0.5 ± 0 | 0.67 ± 0.24 | 0.38 ± 0.29 | 0<.0001 |
| t-tau in pg/ml | 75 ± 31 (N = 25) | 95 ± 59 (N = 44) | 127 ± 40 (N = 23) | 97 ± 52 (N = 92) | 0.001 |
| p-tau in pg/ml | 26 ± 13 (N = 25) | 34 ± 19 (N = 46) | 43 ± 17 (N = 24) | 34 ± 18 (N = 95) | 0.003 |
| Subgroups for APOE-allele-status and β-Amyloid-positivity | | | | | |
| APOE ε4 | N = 56 | N = 78 | N = 41 | N = 175 | 0.002 |
| ε4-negative (N) | 39 (69.6 %) | 37 (47.4 %) | 14 (34.1 %) | 90 (51.4 %) | |
| ε4-positive (N) | 17 (30.4 %) | 41 (52.6 %) | 27 (65.9 %) | 85 (48.6 %) | |
| AB | N = 25 | N = 46 | N = 24 | total (N = 95) | 0.0004 |
| AB- (N) | 17 (68 %) | 13 (28.3 %) | 4 (16.7 %) | 34 (35.8 %) | |
| AB+ (N) | 8 (32 %) | 33 (71.7 %) | 20 (83.3 %) | 61 (64.2 %) | |

Subject characteristics with p-values indicating significance of group differences. Data is expressed as mean ± SD except for Gender, APOE-allele status, β-Amyloid-positivity. Subject count is indicated as N. *AB* β-Amyloid 1–42, *AB* + Aβ-positive, *AB-* Aβ-negative, *AD* Alzheimer's Disease, *APOE* apolipoprotein E, *BMI* body mass index, *CDR* clinical dementia rating, *CN* cognitively normal, *MCI* mild cognitive impairment, *MMSE* mini-mental-status exam, *n.s.* not significant, *SD* standard deviation.

### 3.2. VBM structural covariance of hypothalamic volume with gray and white matter volume

Expectedly, group comparisons (ANOVA F-Test) showed the AD typical and highly significant pattern of medial temporal lobe atrophy (see Fig. S1; detailed data not shown).

Detailed results regarding the relationship of HV with GMV and white matter volume (WMV) can be found in Table 2 and Fig. 3.

ANOVA F-Test revealed no group differences regarding the relationship of HV with GMV and WMV (at $p < 0.05$ FWE cluster-level).

Within the entire sample, multiple regression analysis revealed exclusively positive associations ($p < 0.05$ FWE voxel-level corrected) between HV and GMV, respectively WMV. Expectedly, HV was strongly positively associated with mes- and diencephalic GMV peaking within the right thalamus, but also extended towards the medial temporal lobe. Additional associations were found within several lateral temporal and parietal areas, the bilateral insula, orbitofrontal cortex and the

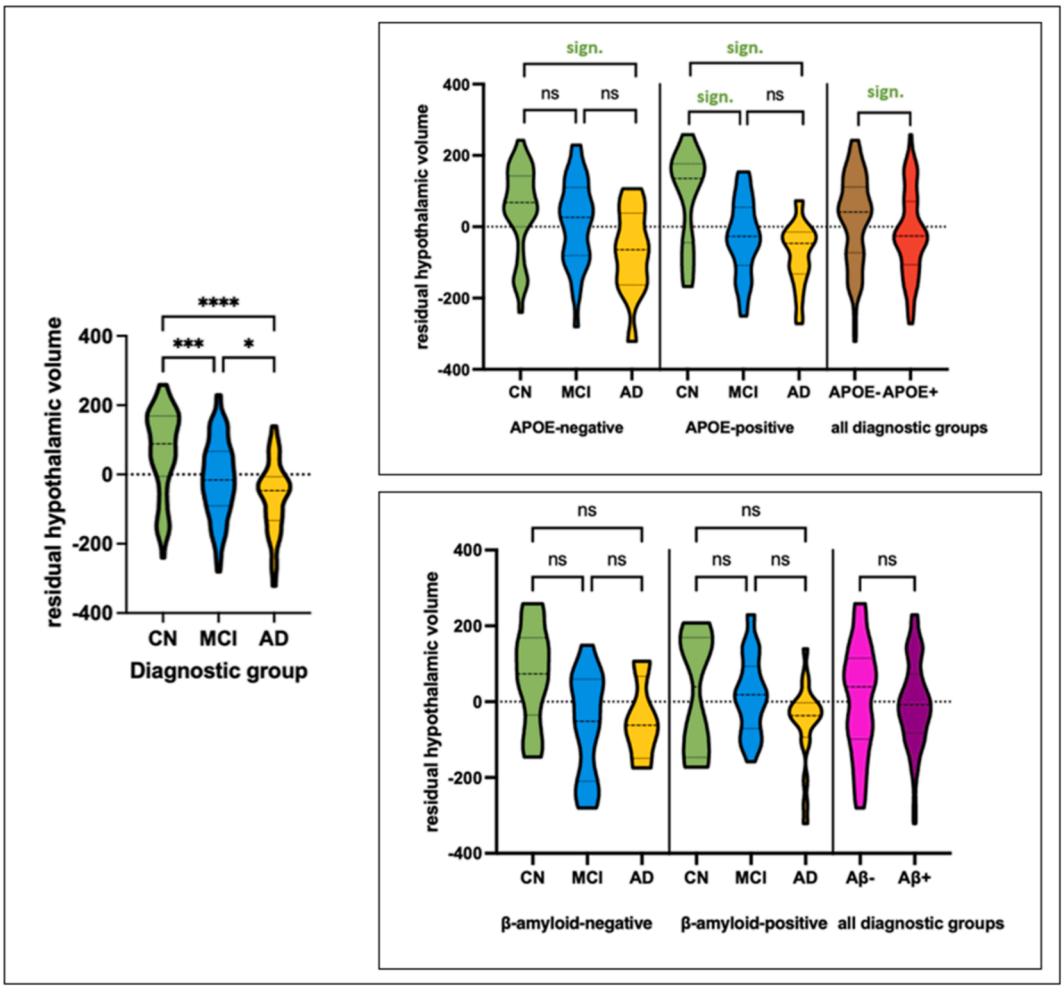


**Fig. 2.** Left: Residualized HV visualised across diagnostic groups showing distribution of HV for cognitively CN subjects, subjects with MCI and AD. Data distribution is visualized using a truncated violin plot with dashed lines indicating median and dotted lines indicating quartiles. Results of pairwise comparison are illustrated with asterisks indicating p-value (ns = P > 0.05; * = P ≤ 0.05; ** = P ≤ 0.01; *** = P ≤ 0.001; **** = P ≤ 0.0001). Right: Residualized HV in APOE- ε*4*-negative vs. APOE- ε*4*-positive subjects and β-amyloid-positive and −negative subjects across diagnostic groups with embedded results of post-hoc Duncan's test showing differences between subgroups. *AD* alzheimer's dementia, APOE apolipoprotein E, *CN* cognitively normal, *HV* hypothalamic volume, *MCI* mild cognitive impairment, *ns* not significant, *sign.* significant.

cerebellum.

For WMV, positive associations of HV were observed with several WM regions, including the corpus callosum and adjacent parts of the fornix, as well as WM within the hippocampal formation.

Overlap of HTH GMV/WMV associations with GMV group differences is illustrated in Fig. S1.

### 3.3. Associations of hypothalamic volume and cortical thickness

Group comparisons (ANOVA F-Test) showed typical patterns of CTH reductions in anterior temporal and – to a lesser degree – the prefrontal cortex (data not shown). Detailed results regarding the relationship of HV with CTH can be found in Table 3 and Fig. 3. ANOVA F-Test revealed no group differences regarding the relationship of HV with CTH ($p < 0.05$ FWE cluster level).

Within the entire sample, multiple regression analysis revealed exclusively positive associations ($p < 0.05$ FWE voxel-level corrected) between HV and CTH, including the right medial OFC, the bilateral occipital cortex (i.e. cuneus), insula, posterior temporomesial regions (i.e. fusiform gyrus), postcentral gyrus, and multiple temporal areas. Overlap of HTH CTH associations with CTH group differences is illustrated in Fig. S1.

### 3.4. Associations of SBM-based networks of structural covariance with hypothalamic volume

For detailed information see Fig. 4. More in depth information on the SBM output including methodological aspects is provided as supplementary material.

Source based morphometry (SBM)-analysis of structural covariance networks (SCN) yielded a total of N = 17 components. Regarding the relationship of HV with SCN we only found a significant group*SCN interaction for the temporomesial component 8 (C8; GLM $p = 0.017$), however this did not remain significant after additional correction for multiple comparisons (i.e. $p > 0.05$ FDR).

Across all groups HV was significantly correlated (pFDR < 0.05; partial Spearman correlation adjusted for TIV, age, gender and diagnostic group) with factor loadings of component 1 (mainly characterized by precuneus and parietal regions), component 3 (mainly characterized by right parietal/temporal regions), component 6 (mainly characterized by anterior cerebellar regions;), component 7 (mainly characterized by frontoinsular regions), component 8 (mainly characterized by temporomesial regions;), component 9 (characterized by thalamic regions), component 12 (mainly characterized by occipital regions), component 14 (mainly characterized by anterior cerebellar regions), component 15 (mainly characterized by left parietal/temporal regions) and component

**Table 2**
Positive associations of hypothalamic volume with gray and white matter volume.

| Regions | p(FWE-corr) | k | T | $MNI_{xyz}$ |
|---|---|---|---|---|
| VBM: Positive associations of hypothalamic volume with gray matter volume | | | | |
| R Thalamus | 0.000 | 35,123 | 9.61 | 6—12 14 |
| R extra-nuclear | 0.000 | | 9.59 | 3—2 −6 |
| L extra-nuclear | 0.000 | | 7.74 | −9—6 −10 |
| R medial frontal gyrus | 0.000 | 2344 | 6.76 | 8 64—16 |
| R rectal gyrus sub-gyral | 0.000 | | 6.56 | 8 40—22 |
| R rectal gyrus frontal lobe | 0.000 | | 6.25 | 9 30—22 |
| R Inferior Semi-Lunar Lobule (Posterior Cerebellum) | 0.000 | 2153 | 6.01 | 24—72 −50 |
| R Pyramis | 0.000 | | 5.97 | 24—78 −40 |
| R Declive | 0.033 | | 4.76 | 22—69 −26 |
| L Inferior Semi-Lunar Lobule (Posterior Cerebellum) | 0.000 | 1307 | 5.92 | −22—78 −50 |
| L Pyramis | 0.000 | | 5.84 | −18—80 −42 |
| L Uvula | 0.011 | | 5.03 | −26—70 −34 |
| L Medial Frontal Gyrus | 0.001 | 929 | 5.71 | −10 30—20 |
| L Sub-Gyral Frontal Lobe | 0.001 | | 5.71 | −18 22—16 |
| L Sub-Gyral Frontal Lobe | 0.009 | | 5.08 | −12 46—20 |
| R postcentral gyrus | 0.002 | 337 | 5.51 | 58—33 42 |
| R postcentral gyrus | 0.017 | | 4.93 | 45—36 50 |
| L Fusiform Gyrus | 0.002 | 582 | 5.47 | −39—66 −21 |
| L Fusiform gyrus | 0.003 | | 5.34 | −44—56 −21 |
| L Inferior temporal gyrus | 0.007 | | 5.15 | −45—45 −24 |
| L Cingulate Gyrus | 0.004 | 142 | 5.29 | −4—39 27 |
| R Inferior Frontal Gyrus | 0.004 | 115 | 5.29 | 36 36—10 |
| L Medial Frontal Gyrus | 0.005 | 29 | 5.24 | −14 51 4 |
| L Superior Temporal Gyrus | 0.005 | 61 | 5.21 | −56—62 18 |
| L Middle Temporal Gyrus | 0.005 | 111 | 5.21 | −66—42 0 |
| R Middle Temporal Gyrus | 0.006 | 83 | 5.18 | 39—75 15 |
| L Paracentral Lobule | 0.006 | 36 | 5.18 | −8—21 50 |
| L Precuneus | 0.007 | 46 | 5.16 | −20—75 39 |
| L Middle Temporal Gyrus | 0.007 | 145 | 5.14 | −60—42 −10 |
| R Superior Temporal Gyrus | 0.007 | 93 | 5.14 | 50 10—26 |
| R Inferior Parietal Lobule | 0.008 | 71 | 5.11 | 66—45 32 |
| R Dorsolateral Prefrontal Cortex | 0.010 | 73 | 5.06 | 40 21 27 |
| L Postcentral Gyrus | 0.012 | 47 | 5.01 | −58—22 24 |
| R Superior Temporal Gyrus | 0.019 | 86 | 4.89 | 30 18—32 |
| L Middle Temporal Gyrus | 0.020 | 18 | 4.89 | −54—70 10 |
| L Precentral Gyrus | 0.023 | 32 | 4.85 | −52—10 32 |
| L Middle Frontal Gyrus | 0.024 | 56 | 4.84 | −27 36—16 |
| R Cingulate Gyrus | 0.025 | 18 | 4.83 | 9—14 44 |
| L Cingulate Gyrus | 0.028 | 15 | 4.80 | −6 8 44 |
| L Postcentral Gyrus | 0.029 | 10 | 4.79 | −66—21 32 |
| VBM: Positive associations of hypothalamic volume with white matter volume | | | | |
| L Corpus Callosum and Fornix | 0.000 | 852 | 5.67 | −4—28 15 |
| R Corpus Callosum and Fornix | 0.001 | | 5.38 | 6—30 15 |
| R Corpus Callosum | 0.003 | 401 | 5.20 | 28—28 −9 |
| R Hippocampus | 0.005 | | 5.10 | 38—24 −14 |
| L Hippocampus | 0.010 | 17 | 4.90 | −30—30 −9 |
| L Corpus Callosum | 0.010 | 64 | 4.89 | 0 33 6 |

Results are listed at $p < 0.05$ (voxel-level FWE-corrected) with corresponding cluster size (k), peak T-value and MNI coordinates. Bold text is used to indicate primary clusters, while secondary peaks within a cluster are not formatted bold. *FWE* family wise error, *L* left, *R* right, *VBM* voxel-based morphometry.

16 (mainly characterized by posterior cerebellar regions) areas. Analyses of individual groups yielded – apart from C8 – largely comparable results with similar directionalities (see Table 4).

With respect to APOE-ε4 carriership, no differences regarding the relationship between HV and SCN were observed (i.e. ε4*SCN interaction term within the GLM).

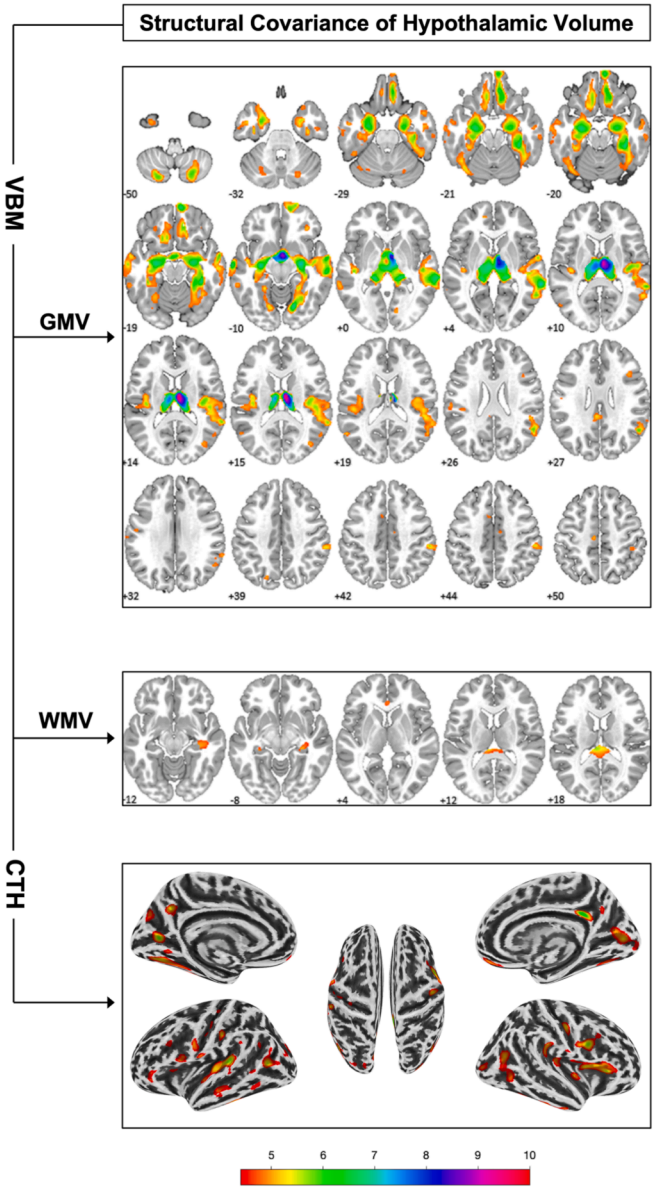


**Fig. 3.** Structural covariance of hypothalamic volume with gray and white matter volume (i.e. GMV, WMV) via voxel-based morphometry (VBM) and with cortical thickness (CTH). Numbers indicate location on the z axis and colours indicate t-score value. Results are illustrated at $p < 0.05$ FWE voxel-level corrected and $k = 10$.

### 3.5. *APOE ε4-allele carriership and structural covariance of hypothalamic volume*

For detailed results regarding the structural covariance of HV in APOE ε4-allele carriers vs. non-carriers please see Fig. 5. In brief, we only found significant results for CTH analyses. Here, ε4-carriership was associated with a weaker association of HV with CTH within the bilateral insular cortex and adjacent temporal regions (left: $MNI_{xyz}$ [-40 mm −8mm −15 mm], pFWEc = 0.01, pFWEp = 0.0, k = 171; right: $MNI_{xyz}$ [38 mm −8mm −6mm], pFWEc = 0.023 pFWEp = 0.06, k = 144].

## 4. Discussion

We investigated HV in a sample of cognitively healthy subjects, subjects with amnestic MCI and dementia due to AD by applying a semi-automated algorithm specifically developed for HTH segmentation.

**Table 3**
Positive associations of hypothalamic volume and cortical thickness.

| Regions | p(FWE-corr) | k | T | $MNI_{xyz}$ |
|---|---|---|---|---|
| R Cingulate Gyrus | 0.000 | 107 | 6.52 | 3—43 30 |
| L Cuneus | 0.000 | 137 | 5.83 | −20—74 6 |
| L Superior Temporal Gyrus | 0.000 | 482 | 5.78 | −46—35 9 |
| L Transverse Temporal Gyrus | 0.001 | | 5.35 | −45—23 9 |
| L Superior Temporal Gyrus | 0.003 | | 4.98 | −47—16 −5 |
| R Frontal Operculum | 0.000 | 188 | 5.73 | 39 5 26 |
| R Inferior Frontal Gyrus | 0.002 | | 5.11 | 52 8 31 |
| R Middle Frontal Gyrus | 0.021 | | 4.52 | 38 17 35 |
| L Middle Temporal Gyrus | 0.000 | 132 | 5.58 | −44—66 10 |
| L Middle Temporal Gyrus | 0.024 | | 4.49 | −48—75 12 |
| L Middle Temporal Gyrus | 0.027 | | 4.46 | −46—68 21 |
| R Inferior Frontal Gyrus | 0.000 | 461 | 5.58 | 38 26 6 |
| R Insula | 0.001 | | 5.39 | 35 7 12 |
| R Insula | 0.001 | | 5.31 | 40 17 7 |
| L Precuneus | 0.000 | 85 | 5.44 | −8—57 33 |
| R Precentral Gyrus | 0.001 | 94 | 5.40 | 37—16 36 |
| L Fusiform Gyrus | 0.001 | 247 | 5.36 | −26—68 −6 |
| L Fusiform Gyrus | 0.005 | | 4.90 | −27—56 −13 |
| R Cuneus | 0.001 | 262 | 5.36 | 14—79 11 |
| R Posterior Cingulate | 0.002 | | 5.14 | 17—66 8 |
| R Lingual Gyrus | 0.015 | | 4.61 | 16—93 −3 |
| L Postcentral Gyrus | 0.001 | 78 | 5.34 | −53—24 32 |
| L Fusiform Gyrus | 0.001 | 87 | 5.33 | −46—37 −26 |
| R Middle Temporal Gyrus | 0.001 | 206 | 5.18 | 38—63 16 |
| R Middle Temporal Gyrus | 0.005 | | 4.88 | 48—60 −2 |
| R Middle Temporal Gyrus | 0.012 | | 4.66 | 45—68 5 |
| R Inferior Parietal Lobule | 0.002 | 136 | 5.17 | 50—30 27 |
| R Inferior Parietal Lobule | 0.003 | | 5.04 | 44—34 24 |
| R Orbital Gyrus | 0.002 | 54 | 5.08 | 4 50—21 |
| L Inferior Frontal Gyrus | 0.003 | 76 | 5.05 | −59 5 29 |
| R Insula | 0.003 | 72 | 5.05 | 39—15 −0 |
| R Insula | 0.003 | 104 | 5.04 | 33—29 17 |
| R Fusiform Gyrus | 0.003 | 51 | 5.03 | 47—28 −25 |
| L Superior Temporal Gyrus | 0.004 | 39 | 4.95 | −60—7 8 |
| R Middle Occipital Gyrus | 0.004 | 48 | 4.93 | 29—86 3 |
| L Precentral Gyrus | 0.005 | 110 | 4.91 | −52 11 8 |
| L Cuneus | 0.005 | 82 | 4.88 | −17—77 29 |
| L Middle Temporal Gyrus | 0.005 | 93 | 4.86 | −58—22 −13 |
| L Middle Temporal Gyrus | 0.022 | | 4.51 | −65—20 −17 |
| R Fusiform Gyrus | 0.006 | 71 | 4.83 | 28—66 −9 |
| R Inferior Temporal Gyrus | 0.006 | 49 | 4.83 | 50—7 −39 |
| R Inferior Temporal Gyrus | 0.033 | | 4.39 | 47—17 −35 |
| L Inferior Frontal Gyrus | 0.010 | 60 | 4.72 | −47 40—12 |
| L Middle Frontal Gyrus | 0.011 | | 4.69 | −49 36—4 |
| L Lingual Gyrus | 0.010 | 29 | 4.72 | −10—61 −3 |
| R Precuneus | 0.011 | 24 | 4.68 | 6—56 34 |
| L Superior Temporal Gyrus | 0.013 | 19 | 4.65 | −42—59 27 |
| L Dorso-lateral Prefrontal Cortex | 0.014 | 27 | 4.62 | −38 20 28 |
| L Cuneus | 0.015 | 35 | 4.61 | −20—87 21 |
| L Middle Temporal Gyrus | 0.016 | 19 | 4.59 | −59—57 6 |
| L Middle Temporal Gyrus | 0.016 | 38 | 4.58 | −57—57 −14 |
| L Middle Occipital Gyrus | 0.017 | 37 | 4.57 | −31—84 14 |
| L Postcentral Gyrus | 0.018 | 25 | 4.56 | –32—28 49 |
| L Superior Frontal Gyrus | 0.018 | 14 | 4.56 | −4 57—20 |
| R Fusiform Gyrus | 0.019 | 21 | 4.55 | 42—49 −15 |
| L Insula | 0.020 | 15 | 4.53 | –32 21 11 |
| R Postcentral Gyrus | 0.028 | 12 | 4.44 | 66—11 15 |
| L Precentral Gyrus | 0.031 | 23 | 4.41 | −35—20 38 |
| L Supramarginal Gyrus | 0.032 | 11 | 4.41 | −60—45 31 |
| L Precentral Gyrus | 0.033 | 10 | 4.40 | −45—13 29 |

Results are listed at $p < 0.05$ (voxel-level FWE-corrected) with corresponding cluster size (k), peak T-value and MNI coordinates. Bold text is used to indicate primary clusters, while secondary peaks within a cluster are not formatted bold. *FWE* family wise error, *L* left, *R* right.

Furthermore, we investigated brain structural covariance of the HTH with VBM based gray and white matter volume and CTH analyses. In a more data-driven approach we made use of SBM to investigate the associations of HV with structural covariance networks. Overall, our results show early hypothalamic atrophy in AD and structural covariance between HV and typical AD-vulnerable regions. Furthermore, we found these results to be somewhat more pronounced in APOE ε4-allele carriers. In turn, HV was not correlated with neither CSF-AB nor BMI or weight change in our cohort.

In AD, involvement of the HTH has been increasingly recognized as potential cause for metabolic and endocrine changes which may potentially further amplify the disease's neuropathological underpinnings (Ishii and Iadecola 2015). So far, relatively few volumetric studies have investigated structural changes of the HTH in AD, likely due to the inherent difficulties in accurately identifying the HTH and measuring its volume. One study using manual segmentation with ROI tracing found hypothalamic atrophy in AD compared to healthy controls (Callen et al. 2001). Using fully automated VBM analysis pipelines, several studies have described hypothalamic involvement in brain atrophy due to AD including its presymptomatic stages, e.g. Hall et al. (2008). Interestingly, Loskutova et al. (2010) found reduced bone density in AD to be associated with HV, indicating that AD related hypothalamic involvement may cause systemic metabolic alterations.

Our study provides additional support regarding early hypothalamic involvement in AD. Here, we found significant differences in HV indicative of increasing hypothalamic atrophy as the disease advances. Importantly, since we found significant reductions of HV in MCI and AD as compared to CN, our findings also indicate early involvement of the HTH in non-dementia stages of AD.

Of note, we applied a validated semi-automated approach which combines ROI-based manual segmentation with automated calculation of HV using seed-growing technology, thus largely avoiding methodological pitfalls of common structural imaging methods such as VBM, which suffer from difficulties in accurately measuring subcortical structures (Bergouignan et al. 2009). Importantly, segmentation issues have been reported when using VBM for HTH volumetry in the AD brain. For instance, Baron et al. (2001) encountered a segmentation issue where nonbrain tissue around the venous sinuses was falsely included as GM. Karas et al. (2003) further classified this problem to be the result of smoothing and identified the ventricles to be especially prone to this error. The HTH is bordering the third ventricle; hence it may be affected by this misclassification error which could lead to overestimation of HV. This proves to be particularly problematic in AD as ventricular enlargement is common. As an alternative to VBM a new automated algorithm for segmentation of the HTH and its subunits based on deep-learning algorithms has been proposed by Billot et al. (2020). Indeed, we did resegment the hypothalami of our sample using the automatic method proposed by Billot et al. and found a moderate correlation between measurements (rho = 0.57). Considering the apparent differences between these measures of HV, further research regarding pitfalls in hypothalamic volumetry with semi-automated and fully automated methods might be needed.

Nonetheless manual segmentation is still considered the gold standard in hypothalamic volumetry and studies which investigated HV with a manual algorithm obtained highly accurate results (Schindler et al. 2013; Billot et al. 2020; Ali et al. 2022). Yet, manual segmentation is often time consuming and can be less accessible (i.e. 7 T MRI required (Schindler et al. 2013)) which is why we chose a validated semi-automated approach in our study (Wolff et al. 2018). The use of GM-TPM-guided anatomical landmarks allows for correct and precise identification of hypothalamic voxels and manual review of the segmentation result is possible while the use of seed growing technique makes the segmentation process more efficient. Thus, the method we chose for hypothalamic volumetry is a major strength of our study.

Investigating the relationship of APOE ε4-allele carriership and HV, we did find significant group differences regarding HV in both ε4-positive and ε4-negative subjects, while group differences were more pronounced in APOE ε4-carriers. APOE ε4 carriership in AD has been associated with accelerated clinical progression in some cohorts (Sando et al. 2008; Qian et al. 2021; Suzuki et al. 2020) as well as faster spread of amyloid and tau pathology and brain metabolic alterations (Murphy et al. 2013; Steward et al. 2023). Considering this, APOE ε4 could have also promoted accelerated neurodegeneration of the hypothalamus in subjects with MCI and AD in our cohort, which could explain why

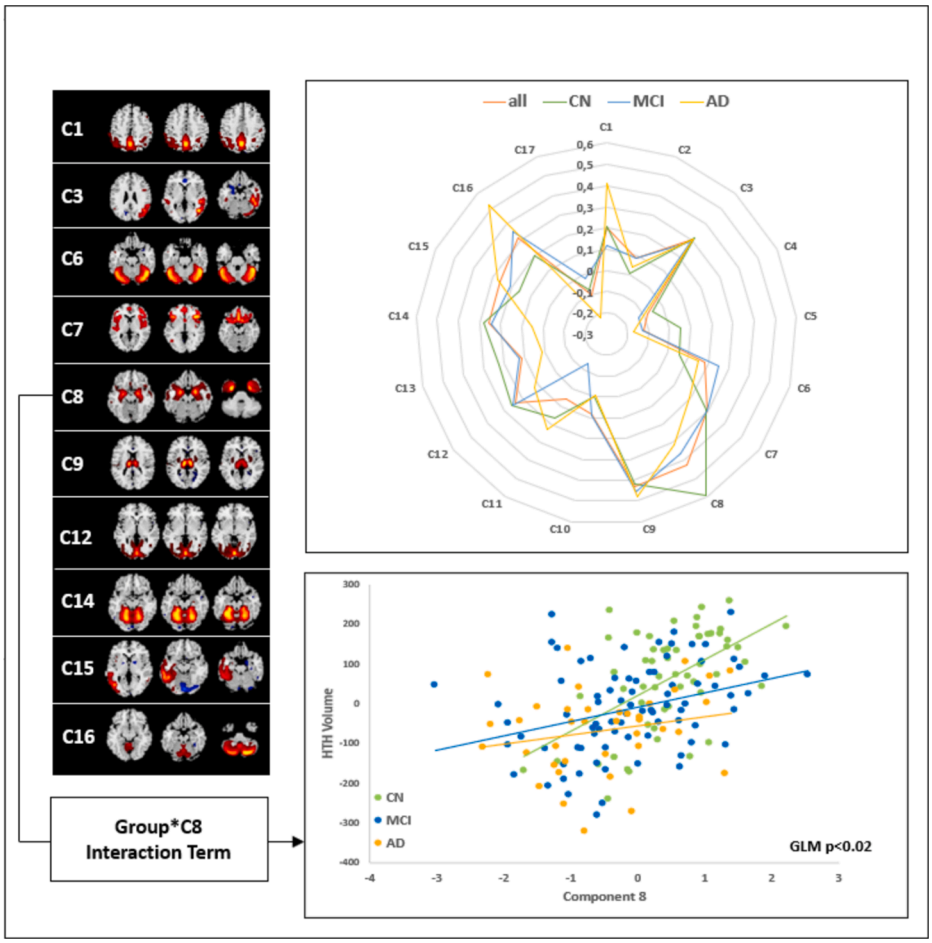


**Fig. 4.** Radar chart illustrating the correlations (i.e. Spearman rho) between hypothalamic volume (HV) and individual source-based morphometry (SBM)-based structural covariance networks across diagnostic groups and within the entire sample. Components significantly correlated with HV (i.e. whole sample; pFDR < 0.05) are shown to the left with yellow/red indicating positive covariation and blue colours indicating negative covariation. Scatter plot illustrates the relationship between HV and temporomesial component 8 (C8) and the trend-level significant ($p < 0.05$ uncorrected) Group*C8 interaction term. *HTH* hypothalamus. (For interpretation of the references to colour in this figure legend, the reader is referred to the web version of this article.)

**Table 4**
Partial correlations of hypothalamic volume with gray matter structural covariance networks across diagnostic groups.

| SBM Components | Group Pooledrho | pFDR | CN rho | pFDR | MCI rho | pFDR | AD rho | pFDR |
|---|---|---|---|---|---|---|---|---|
| C1 | 0.20 | 0.02 | 0.21 | n.s. | 0.12 | n.s. | 0.41 | n.s. |
| C2 | 0.08 | n.s. | 0.01 | n.s. | 0.08 | n.s. | 0.04 | n.s. |
| C3 | 0.31 | 0<.001 | 0.31 | n.s. | 0.30 | 0.04 | 0.30 | n.s. |
| C4 | −0.08 | n.s. | −0.06 | n.s. | −0.13 | n.s. | −0.10 | n.s. |
| C5 | −0.12 | n.s. | 0.05 | n.s. | −0.13 | n.s. | −0.17 | n.s. |
| C6 | 0.18 | 0.03 | 0.06 | n.s. | 0.25 | n.s. | 0.15 | n.s. |
| C7 | 0.30 | 0<.001 | 0.29 | n.s. | 0.30 | 0.04 | 0.19 | n.s. |
| C8 | 0.43 | 0<.001 | 0.59 | 0.002 | 0.36 | 0.011 | 0.31 | n.s. |
| C9 | 0.43 | 0<.001 | 0.42 | 0.015 | 0.46 | 0.002 | 0.48 | 0.019 |
| C10 | 0.08 | n.s. | 0.00 | n.s. | 0.09 | n.s. | −0.01 | n.s. |
| C11 | 0.06 | n.s. | 0.16 | n.s. | −0.14 | n.s. | 0.23 | n.s. |
| C12 | 0.24 | 0.004 | 0.26 | n.s. | 0.25 | n.s. | 0.12 | n.s. |
| C13 | 0.12 | n.s. | 0.23 | n.s. | 0.13 | n.s. | 0.01 | n.s. |
| C14 | 0.26 | 0.002 | 0.28 | n.s. | 0.24 | n.s. | 0.05 | n.s. |
| C15 | 0.26 | 0.002 | 0.16 | n.s. | 0.21 | n.s. | 0.27 | n.s. |
| C16 | 0.31 | 0<.001 | 0.20 | n.s. | 0.35 | 0.011 | 0.52 | 0.014 |
| C17 | −0.10 | n.s. | −0.08 | n.s. | −0.02 | n.s. | −0.22 | n.s. |

Partial spearman correlations (rho) of structural covariance network loading coefficients with hypothalamic volume across diagnostic groups [all partial spearman correlations adjusted for TIV, age, gender and diagnostic groups (pooled group only)]. Results are listed at $p < 0.05$ False Discovery Rate (FDR) corrected; *n.s.* not statistically significant; *CN* cognitively normal; *MCI* mild cognitive impairment; *AD* alzheimer's dementia; *SBM* source-based morphometry.

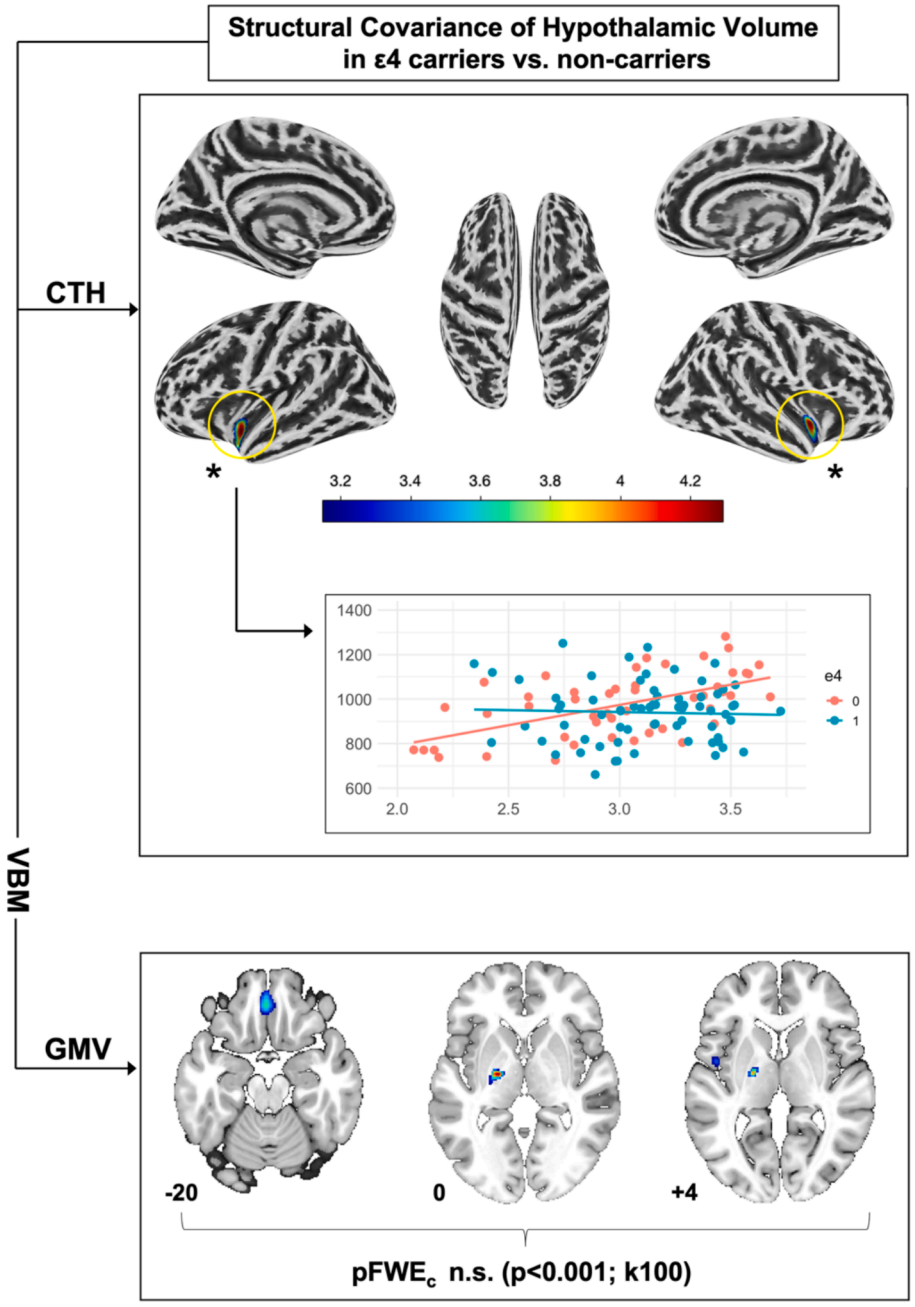


**Fig. 5.** Structural covariance of hypothalamic volume (HV) with cortical thickness (CTH) and gray matter volume (GMV) depending on apolipoprotein E (APOE) ε4-allele carriership. Numbers indicate location on the z axis and colour indicates t-score value. ε4 = 1 homo- or heterozygous carriership of APOE ε4-allele, ε4 = 0 no APOE ε4-allele carriership. Results of CTH analyses are illustrated at $p < 0.05$ family-wise error (FWE) voxel-level corrected and $k = 10$. Voxel-based morphometry (VBM) GMV analyses are illustrated at a liberal, uncorrected threshold of $p < 0.001$ and $k = 100$.

changes would be more pronounced in APOE ε4-carriers.

In a subsample (N = 95) with available CSF data, we did not find significant differences of HV between AB+ vs. AB- subjects. It needs to be noted though, that these results are based on pooled samples due to small sample sizes, although diagnostic groups were taken into account. Formation of AB plaques (Ogomori et al. 1989; Standaert et al. 1991) and neurodegeneration (Ogomori et al. 1989; Standaert et al. 1991; Baloyannis et al. 2015; Baloyannis et al. 2016) have been shown to affect the HTH of AD patients. Yet, MRI-measured atrophy does not always seem to correlate with amyloid distribution in the AD brain. Jack et al. (2013), for instance, found brain atrophy to correlate only with distribution of neurofibrillary tangles (NFT) not AB, showing that tau-mediated neurodegeneration might have more impact on volumetric changes. Studies correlating CSF-t-tau and p-tau with regional and whole brain atrophy in AD have been reporting mixed results (Schönknecht et al. 2003; Sluimer et al. 2010; Tarawneh et al. 2015; Llibre-Guerra et al. 2019; Contador et al. 2021). In our study, we did not find a significant correlation of total HV with CSF t-tau/p-tau. Overall, our results do not support a strong relationship of AD biomarker status with hypothalamic atrophy.

Considering metabolic impacts, we investigated correlations of HV with BMI and longitudinal weight changes yet did not find significant associations. Previous VBM studies in obese but neurologically healthy humans found contradicting results regarding the association of HV with BMI (Horstmann et al. 2011; Kurth et al. 2013). Using the same semi-automated algorithm for HTH volumetry as in our study, Thomas

et al. (2019) also found no correlation between HV and BMI. Instead, they found associations of BMI with microstructural changes in the HTH with diffusion tensor imaging (DTI). Spindler et al. (2020) also discovered a significant association of BMI and mean diffusivity (MD) within the anterior–superior HTH in a large sample of healthy subjects. This could be an indicator that volumetry might be limited in detecting subtle hypothalamic changes in AD, which in turn could have limited our results.

As a homeostatic and autonomic key structure, the HTH is densely connected not only within the Papez circuit but throughout the entire CNS. On the topic of neural networks, Kim et al. (2022) investigated the alteration of large neural circuits in AD, which connect the hippocampus, thalamus, and HTH with septal, olfactory, visual, and other limbic brain areas and influence AD pathology and clinical manifestation. They argue that impaired connectivity between these areas could help explain many of the symptoms of AD and possibly provide new therapeutic targets. Therefore, we additionally investigated hypothalamic structural covariance with the entire brain. Structural covariance analyses – both seed based and SBM based – have shown to reliably provide information regarding the structural organization of the brain on a network level (Xu et al. 2009; DuPre and Spreng 2017). Across the entire sample, we observed comparable results in GMV, CTH and SBM structural covariance analyses, with HV being associated with widespread parts of the brain, most significantly however the hippocampal region, next to neighbouring subcortical mes- and diencephalic structures. While analyses of GMV showed substantial overlap with disease related atrophy (see Fig. S1), CTH analyses only yielded smaller overlapping regions within the posterior cingulum and the left temporal lobe. While the HTHs dense connections that include brain regions not primarily affected by AD may have contributed to this observation, it must be noted that CTH – in contrast to VBM based analyses of GMV – captures only one aspect of brain morphology.

Considering potential diverging and group specific relationships of HV with brain structural parameters (i.e. group*HTH Interaction term) no significant results were found in VBM and CTH analyses. Only our SBM analyses point to an attenuated association of HV with the hippocampal region in humans with more advanced disease stages, although this observation did not reach significance when taking multiple comparisons into account (i.e. $p > 0.05$ after FDR correction). Nevertheless, considering the critical role of the hippocampus in AD these results seem plausible and may be explained by increasing hippocampal atrophy and a delayed – and potentially secondary – atrophy of the HTH. The hippocampus is a pivotal brain structure with regards to episodic and spatial memory (Maguire et al. 2000; Di Paola et al. 2007), thus its early affection in AD contributes to episodic memory loss. However, moving away from a hippocampus-centred understanding of the disease, some authors argue that deficits of episodic and spatial memory in AD can only be fully understood by including other structures of the Papez circuit and their interconnections in future analyses (Di Paola et al. 2007; Forno et al. 2021; Aggleton et al. 2022). Under this consideration we also investigated VBM-based associations of HV with WMV. Although again, no significant group*HTH interaction term was observed, we did find a positive association of HV with fornix WMV within the entire sample. Several authors have previously found atrophy of the fornix in AD which has been associated with changes in hippocampal volume and clinical manifestations of AD (Callen et al. 2001; Copenhaver et al. 2006). We speculate that hippocampal atrophy in AD might contribute to atrophy of the fornix which in turn may cause secondary atrophy of the HTH. Additionally, a primarily neurodegenerative genesis of hypothalamic atrophy in AD is also possible since neurodegeneration in AD spreads across the brain following Braak's stages. From the hippocampus, which is affected in the early entorhinal stage, tau-mediated neurodegeneration is postulated to spread across the brain transneuronally (Vogel et al. 2020), thus areas connected to the hippocampus, like the HTH, are likely to be affected as well. To summarize, both secondary atrophy following hippocampal atrophy as well as atrophy resulting from tau-mediated neurodegeneration in AD are possible causes for hypothalamic atrophy in AD and future research should address potential mechanisms involved.

Hypothalamic dysfunction has been discussed as a driver of noncognitive and metabolic AD symptoms like late-life weight loss, reduced bone density and circadian disruption (Loskutova et al. 2010; Ishii and Iadecola 2015; Hiller and Ishii 2018), thus further investigations of hypothalamic involvement in AD might help discover new therapeutic targets. Since metabolic alterations have been shown to have multiple adverse effects in AD (Loskutova et al. 2009; Burns et al. 2010; Pillai et al. 2023) and considering that our data indicate early involvement of the HTH, therapeutic approaches specifically targeting hypothalamic function in early disease stages could have implications for disease progression and the overall prognosis. However, while there have been pharmacological as well as interventional approaches targeting disrupted hypothalamic pathways in AD mouse models, like leptin therapy (Tezapsidis et al. 2009; Greco et al. 2010), glucocorticoid receptor antagonists (Lesuis et al. 2018) or light flicker stimulation of the central clock in suprachiasmatic neurons (Yao et al. 2020), promising studies in humans are still missing.

Our study has several limitations. First, this is a secondary analysis of pre-existing data with only limited AD biomarker data for our subsample. Nevertheless, the data we used were acquired following strict and optimized protocols of clinical diagnosis and image acquisition. Of note, ADNI used a clinical approach for diagnosis (McKhann et al. 1984; Petersen et al. 2010), yet current diagnostic consensus guidelines highlight the necessity of fluid or imaging biomarker positivity to accurately diagnose AD (Dubois et al. 2021). Interpreting biomarker-negative AD is challenging, yet in amyloid-negative subjects with clinical AD, cognitive decline may be caused by other pathologies such as vascular disease, depression (Landau et al. 2016; Jack et al. 2016) or other neurodegenerative diseases (e.g. LATE; limbic-predominant age-related TDP-43 encephalopathy; Nelson et al. 2019). For our study, CSF AD biomarker data were available in a subsample only with some participants being categorized as AB- MCI or AD. Albeit limited by small sample sizes, corresponding analyses of HV in AB- and AB+ subsamples do support the findings from our main analyses. Still, in light of this limitation, the results of our study should be interpreted with caution and reproduced in more detailed characterized populations. Another limitation is the cross-sectional and purely associative design of our study, which does not allow claims of causality. Although our volumetric approach is accurate, it does not allow for segmentation of individual hypothalamic nuclei which might provide further functional insight into hypothalamic involvement in AD than just volumetry of the whole HTH. Lastly, we used VBM for analysis of gray and white matter covariance, which can have limited spatial resolution regarding small subcortical structures. Particularly for white matter changes, more accurate measures like DTI are required to provide additional and more in-depth insight.

## 5. Conclusions

To summarize, we found increasing hypothalamic atrophy from early, non-dementia stages (i.e. amnestic MCI) towards dementia stages of AD in comparisons to healthy controls. While HV showed strong structural covariance with structures typically affected by MCI and AD, our findings suggest that AD related atrophy of the hippocampus and structures of the Papez circuit could promote secondary atrophy of the HTH. Future studies are required to evaluate additional contributions of AD pathology.

Consent statement

All participants gave informed consent through their local IRBs prior to study participation. Within the ADNI protocol, all procedures involving human participants were in accordance with the 1964 Helsinki declaration and its later amendments (for details see https://www.adni.loni.usc.edu). Data are available from the corresponding author on

reasonable request.

## CRediT authorship contribution statement

**Hannah Pecher:** Writing – original draft, Visualization, Validation, Methodology, Investigation, Formal analysis, Data curation. **Melanie Storch:** Writing – review & editing, Methodology. **Frauke Beyer:** Writing – review & editing, Software, Methodology. **Veronica Witte:** Writing – review & editing, Software. **Christian-Frank Baasner:** Writing – review & editing, Methodology. **Peter Schönknecht:** Writing – review & editing, Software, Methodology. **Christopher M. Weise:** Writing – review & editing, Visualization, Validation, Supervision, Project administration, Investigation, Formal analysis, Data curation, Conceptualization.

## Declaration of competing interest

The authors declare that they have no known competing financial interests or personal relationships that could have appeared to influence the work reported in this paper.

## Acknowledgements

Data collection and sharing for this project was funded by the Alzheimer's Disease Neuroimaging Initiative (ADNI) (National Institutes of Health Grant U01 AG024904) and DOD ADNI (Department of Defense award number W81XWH-12-2-0012). ADNI is funded by the National Institute on Aging, the National Institute of Biomedical Imaging and Bioengineering, and through generous contributions from the following: AbbVie, Alzheimer's Association; Alzheimer's Drug Discovery Foundation; Araclon Biotech; BioClinica, Inc.; Biogen; Bristol-Myers Squibb Company; CereSpir, Inc.; Cogstate; Eisai Inc.; Elan Pharmaceuticals, Inc.; Eli Lilly and Company; EuroImmun; F. Hoffmann-La Roche Ltd and its affiliated company Genentech, Inc.; Fujirebio; GE Healthcare; IXICO Ltd.;Janssen Alzheimer Immunotherapy Research & Development, LLC.; Johnson & Johnson Pharmaceutical Research & Development LLC.; Lumosity; Lundbeck; Merck & Co., Inc. ;Meso Scale Diagnostics, LLC.; NeuroRx Research; Neurotrack Technologies; Novartis Pharmaceuticals Corporation; Pfizer Inc.; Piramal Imaging; Servier; Takeda Pharmaceutical Company; and Transition Therapeutics. The Canadian Institutes of Health Research is providing funds to support ADNI clinical sites in Canada. Private sector contributions are facilitated by the Foundation for the National Institutes of Health (www.fnih.org). The grantee organization is the Northern California Institute for Research and Education, and the study is coordinated by the Alzheimer's Therapeutic Research Institute at the University of Southern California. ADNI data are disseminated by the Laboratory for Neuro Imaging at the University of Southern California.

The funding sources had no role in the preparation of the article, study design, collection, analysis and interpretation of data, writing of the report and decision to submit the article for publication.

## Appendix A. Supplementary data

Supplementary data to this article can be found online at https://doi.org/10.1016/j.nicl.2024.103687.

## Data availability

Data will be made available on request.

## References

Aggleton, J.P., Nelson, A.J.D., O'Mara, S.M., 2022. Time to retire the serial Papez circuit: Implications for space, memory, and attention. Neuroscience and Biobehavioral Reviews 140, 104813. https://doi.org/10.1016/j.neubiorev.2022.104813.

Ali, Mohammad; Suh, Jee Su; Ramonas, Milita; Hassel, Stefanie; Arnott, Stephen R.; Strother, Stephen C. et al. (2022): A detailed manual segmentation procedure for the hypothalamus for 3T T1-weighted MRI. In *MethodsX* 9, p. 101864. DOI: 10.1016/j.mex.2022.101864.

Ashburner, J., Friston, K.J., 2000. Voxel-based morphometry–the methods. NeuroImage 11 (6 Pt 1), 805–821. https://doi.org/10.1006/nimg.2000.0582.

Baloyannis, S.J., Mavroudis, I., Mitilineos, D., Baloyannis, I.S., Costa, V.G., 2015. The hypothalamus in Alzheimer's disease: a Golgi and electron microscope study. American Journal of Alzheimer's Disease and Other Dementias 30 (5), 478–487. https://doi.org/10.1177/1533317514556876.

Baloyannis, S.J., Mavroudis, I., Baloyannis, I.S., Costa, V.G., 2016. Mammillary Bodies in Alzheimer's Disease: A Golgi and Electron Microscope Study. American Journal of Alzheimer's Disease and Other Dementias 31 (3), 247–256. https://doi.org/10.1177/1533317515602548.

Baron, J.C., Chételat, G., Desgranges, B., Perchey, G., Landeau, B., de La Sayette, V., Eustache, F., 2001. In vivo mapping of gray matter loss with voxel-based morphometry in mild Alzheimer's disease. NeuroImage 14 (2), 298–309. https://doi.org/10.1006/nimg.2001.0848.

Bergouignan, L., Chupin, M., Czechowska, Y., Kinkingnéhun, S., Lemogne, C., Bastard, L. E., Guillaume, et al., 2009. Can voxel based morphometry, manual segmentation and automated segmentation equally detect hippocampal volume differences in acute depression? NeuroImage 45 (1), 29–37. https://doi.org/10.1016/j.neuroimage.2008.11.006.

Billot, B., Bocchetta, M., Todd, E., Dalca, A.V., Rohrer, J.D., Iglesias, J.E., 2020. Automated segmentation of the hypothalamus and associated subunits in brain MRI. NeuroImage 223. https://doi.org/10.1016/j.neuroimage.2020.117287.

Braak, H., Braak, E., 1991. Neuropathological stageing of Alzheimer-related changes. Acta Neuropathol 82 (4), 239–259. https://doi.org/10.1007/BF00308809.

Burns, J.M., Johnson, D.K., Watts, A., Swerdlow, R.H., Brooks, W.M., 2010. Reduced lean mass in early Alzheimer disease and its association with brain atrophy. Archives of Neurology 67 (4), 428–433. https://doi.org/10.1001/archneurol.2010.38.

Callen, D.J., Black, S.E., Gao, F., Caldwell, C.B., Szalai, J.P., 2001. Beyond the hippocampus: MRI volumetry confirms widespread limbic atrophy in AD. Neurology 57 (9), 1669–1674. https://doi.org/10.1212/wnl.57.9.1669.

Choi, S.-H., Kim, Y.-B., Paek, S.-H., Cho, Z.-H., 2019. Papez Circuit Observed by in vivo Human Brain With 7.0T MRI Super-Resolution Track Density Imaging and Track Tracing. Frontiers in Neuroanatomy 13, 17. https://doi.org/10.3389/fnana.2019.00017.

Colliot, O., Chételat, G., Chupin, M., Desgranges, B., Magnin, B., Benali, H., et al., 2008. Discrimination between Alzheimer disease, mild cognitive impairment, and normal aging by using automated segmentation of the hippocampus. Radiology 248 (1), 194–201. https://doi.org/10.1148/radiol.2481070876.

Contador, J., Pérez-Millán, A., Tort-Merino, A., Balasa, M., Falgàs, N., Olives, J., et al., 2021. Longitudinal brain atrophy and CSF biomarkers in early-onset Alzheimer's disease. NeuroImage. Clinical 32, 102804. https://doi.org/10.1016/j.nicl.2021.102804.

Copenhaver, B.R., Rabin, L.A., Saykin, A.J., Roth, R.M., Wishart, H.A., Flashman, L.A., et al., 2006. The fornix and mammillary bodies in older adults with Alzheimer's disease, mild cognitive impairment, and cognitive complaints: a volumetric MRI study. Psychiatry Research 147 (2–3), 93–103. https://doi.org/10.1016/j.pscychresns.2006.01.015.

Dahnke, R., Yotter, R., Aine; Gaser, Christian, 2013. Cortical thickness and central surface estimation. NeuroImage 65, 336–348. https://doi.org/10.1016/j.neuroimage.2012.09.050.

Di Paola, M., Macaluso, E., Carlesimo, G.A., Tomaiuolo, F., Worsley, K.J., Fadda, L., Caltagirone, C., 2007. Episodic memory impairment in patients with Alzheimer's disease is correlated with entorhinal cortex atrophy. A voxel-based morphometry study. In. Journal of Neurology 254 (6), 774–781. https://doi.org/10.1007/s00415-006-0435-1.

Dubois, B., Villain, N., Frisoni, G.B., Rabinovici, G.D., Sabbagh, M., Cappa, S., et al., 2021. Clinical diagnosis of Alzheimer's disease: recommendations of the International Working Group. the Lancet. Neurology 20 (6), 484–496. https://doi.org/10.1016/S1474-4422(21)00066-1.

DuPre, E., Spreng, R.N., 2017. Structural covariance networks across the life span, from 6 to 94 years of age. Network Neuroscience (cambridge, Mass.) 1 (3), 302–323. https://doi.org/10.1162/netn_a_00016.

Edwards, I.I.I., George, A., Gamez, N., Escobedo, G., Calderon, O., Moreno-Gonzalez, I., 2019. Modifiable Risk Factors for Alzheimer's Disease. Frontiers in Aging Neuroscience 11, 146. https://doi.org/10.3389/fnagi.2019.00146.

Evans, A.C., 2013. Networks of anatomical covariance. In. NeuroImage 80, 489–504. https://doi.org/10.1016/j.neuroimage.2013.05.054.

Folstein, M.F., Folstein, S.E., McHugh, P.R., 1975. "Mini-mental state". A practical method for grading the cognitive state of patients for the clinician. In. Journal of Psychiatric Research 12 (3), 189–198. https://doi.org/10.1016/0022-3956(75)90026-6.

Forno, G., Lladó, A., Hornberger, M., 2021. Going round in circles-The Papez circuit in Alzheimer's disease. the European Journal of Neuroscience 54 (10), 7668–7687. https://doi.org/10.1111/ejn.15494.

Greco, S.J., Bryan, K.J., Sarkar, S., Zhu, X., Smith, M.A., Ashford, J.W., et al., 2010. Leptin reduces pathology and improves memory in a transgenic mouse model of Alzheimer's disease. Journal of Alzheimer's Disease: JAD 19 (4), 1155–1167. https://doi.org/10.3233/JAD-2010-1308.

Hall, A.M., Moore, R.Y., Lopez, O.L., Kuller, L., Becker, J.T., 2008. Basal forebrain atrophy is a presymptomatic marker for Alzheimer's disease. Alzheimer's & Dementia: The Journal of the Alzheimer's Association 4 (4), 271–279. https://doi.org/10.1016/j.jalz.2008.04.005.

Hiller, A.J., Ishii, M., 2018. Disorders of Body Weight, Sleep and Circadian Rhythm as Manifestations of Hypothalamic Dysfunction in Alzheimer's Disease. Frontiers in Cellular Neuroscience 12, 471. https://doi.org/10.3389/fncel.2018.00471.

Horstmann, A., Busse, F.P., Mathar, D., Müller, K., Lepsien, J., Schlögl, H., et al., 2011. Obesity-related differences between women and men in brain structure and goal-directed behavior. Frontiers in Human Neuroscience 5, 58. https://doi.org/10.3389/fnhum.2011.00058.

Hughes, C.P., Berg, L., Danziger, W.L., Coben, L.A., Martin, R.L., 1982. A new clinical scale for the staging of dementia. the British Journal of Psychiatry : the Journal of Mental Science 140, 566–572. https://doi.org/10.1192/bjp.140.6.566.

Ishii, M., Iadecola, C., 2015. Metabolic and Non-Cognitive Manifestations of Alzheimer's Disease: The Hypothalamus as Both Culprit and Target of Pathology. Cell Metabolism 22 (5), 761–776. https://doi.org/10.1016/j.cmet.2015.08.016.

Jack, C.R., Knopman, D.S., Jagust, W.J., Petersen, R.C., Weiner, M.W., Aisen, P.S., et al., 2013. Tracking pathophysiological processes in Alzheimer's disease: an updated hypothetical model of dynamic biomarkers. Lancet Neurology 12 (2), 207–216. https://doi.org/10.1016/S1474-4422(12)70291-0.

Jack, C.R., Knopman, D.S., Chételat, G., Dickson, D., Fagan, A.M., Frisoni, G.B., et al., 2016. Suspected non-Alzheimer disease pathophysiology–concept and controversy. Nature Reviews. Neurology 12 (2), 117–124. https://doi.org/10.1038/nrneurol.2015.251.

Karas, G.B., Burton, E.J., Rombouts, S.A.R.B., van Schijndel, R.A., O'Brien, J.T., Scheltens, P.H., et al., 2003. A comprehensive study of gray matter loss in patients with Alzheimer's disease using optimized voxel-based morphometry. NeuroImage 18 (4), 895–907. https://doi.org/10.1016/s1053-8119(03)00041-7.

Kim, Sujin; Nam, Yunkwon; Kim, Hyeon Soo; Jung, Haram; Jeon, Seong Gak; Hong, Sang Bum; Moon, Minho (2022): Alteration of Neural Pathways and Its Implications in Alzheimer's Disease. In *Biomedicines* 10 (4). DOI: 10.3390/biomedicines10040845.

Kurth, F., Levitt, J.G., Phillips, O.R., Luders, E., Woods, R.P., Mazziotta, J.C., et al., 2013. Relationships between gray matter, body mass index, and waist circumference in healthy adults. Human Brain Mapping 34 (7), 1737–1746. https://doi.org/10.1002/hbm.22021.

Landau, S.M., Horng, A., Fero, A., Jagust, W.J., 2016. Amyloid negativity in patients with clinically diagnosed Alzheimer disease and MCI. Neurology 86 (15), 1377–1385. https://doi.org/10.1212/WNL.0000000000002576.

Lesuis, S.L., Weggen, S., Baches, S., Lucassen, P.J., Krugers, H.J., 2018. Targeting glucocorticoid receptors prevents the effects of early life stress on amyloid pathology and cognitive performance in APP/PS1 mice. Translational Psychiatry 8 (1), 53. https://doi.org/10.1038/s41398-018-0101-2.

Llibre-Guerra, J.J., Li, Y., Schindler, S.E., Gordon, B.A., Fagan, A.M., Morris, J.C., et al., 2019. Association of Longitudinal Changes in Cerebrospinal Fluid Total Tau and Phosphorylated Tau 181 and Brain Atrophy With Disease Progression in Patients With Alzheimer Disease. JAMA Network Open 2 (12), e1917126.

Loskutova, N., Honea, R.A., Vidoni, E.D., Brooks, W.M., Burns, J.M., 2009. Bone density and brain atrophy in early Alzheimer's disease. Journal of Alzheimer's Disease: JAD 18 (4), 777–785. https://doi.org/10.3233/JAD-2009-1185.

Loskutova, N., Honea, R.A., Brooks, W.M., Burns, J.M., 2010. Reduced limbic and hypothalamic volumes correlate with bone density in early Alzheimer's disease. Journal of Alzheimer's Disease : JAD 20 (1), 313–322. https://doi.org/10.3233/JAD-2010-1364.

Maguire, E.A., Gadian, D.G., Johnsrude, I.S., Good, C.D., Ashburner, J., Frackowiak, R.S., Frith, C.D., 2000. Navigation-related structural change in the hippocampi of taxi drivers. Proceedings of the National Academy of Sciences of the United States of America 97 (8), 4398–4403. https://doi.org/10.1073/pnas.070039597.

McKhann, G., Drachman, D., Folstein, M., Katzman, R., Price, D., Stadlan, E.M., 1984. Clinical diagnosis of Alzheimer's disease: report of the NINCDS-ADRDA Work Group under the auspices of Department of Health and Human Services Task Force on Alzheimer's Disease. Neurology 34 (7), 939–944. https://doi.org/10.1212/WNL.34.7.939.

Mechelli, A., Friston, K.J., Frackowiak, R.S., Price, C.J., 2005. Structural covariance in the human cortex. Journal of Neuroscience : the Official Journal of the Society for Neuroscience 25 (36), 8303–8310. https://doi.org/10.1523/JNEUROSCI.0357-05.2005.

Murphy, K.R., Landau, S.M., Choudhury, K., Roy; Hostage, Christopher A., Shpanskaya, Katie S., Sair, Haris I., et al., 2013. Mapping the effects of ApoE4, age and cognitive status on 18F-florbetapir PET measured regional cortical patterns of beta-amyloid density and growth. NeuroImage 78, 474–480. https://doi.org/10.1016/j.neuroimage.2013.04.048.

Nelson, P.T., Dickson, D.W., Trojanowski, J.Q., Jack, C.R., Boyle, P.A., Arfanakis, K., et al., 2019. Limbic-predominant age-related TDP-43 encephalopathy (LATE): consensus working group report. Brain : a Journal of Neurology 142 (6), 1503–1527. https://doi.org/10.1093/brain/awz099.

Nichols, E., Szoeke, C.E.I., Vollset, S., Emil; Abbasi, Nooshin; Abd-Allah, Foad; Abdela, Jemal, et al., 2019. Global, regional, and national burden of Alzheimer's disease and other dementias, 1990–2016: a systematic analysis for the Global Burden of Disease Study 2016. Lancet Neurology 18 (1), 88–106. https://doi.org/10.1016/S1474-4422(18)30403-4.

Ogomori, K., Kitamoto, T., Tateishi, J., Sato, Y., Suetsugu, M., Abe, M., 1989. Beta-protein amyloid is widely distributed in the central nervous system of patients with Alzheimer's disease. American Journal of Pathology 134 (2), 243–251.

Papez, J.W., 1937. A proposed mechanism of emotion. Arch NeurPsych 38 (4), 725. https://doi.org/10.1001/archneurpsyc.1937.02260220069003.

Petersen, R.C., Aisen, P.S., Beckett, L.A., Donohue, M.C., Gamst, A.C., Harvey, D.J., et al., 2010. Alzheimer's Disease Neuroimaging Initiative (ADNI): clinical characterization. Neurology 74 (3), 201–209. https://doi.org/10.1212/WNL.0b013e3181cb3e25.

Pillai, J.A., Bena, J., Bekris, L., Kodur, N., Kasumov, T., Leverenz, J.B., Kashyap, S.R., 2023. Metabolic syndrome biomarkers relate to rate of cognitive decline in MCI and dementia stages of Alzheimer's disease. Alzheimer's Research & Therapy 15 (1), 54. https://doi.org/10.1186/s13195-023-01203-y.

Prince, M., Bryce, R., Albanese, E., Wimo, A., Ribeiro, W., Ferri, C.P., 2013. The global prevalence of dementia: a systematic review and metaanalysis. Alzheimer's & Dementia: the Journal of the Alzheimer's Association 9 (1), 63–75.e2. https://doi.org/10.1016/j.jalz.2012.11.007.

Qian, J., Betensky, R.A., Hyman, B.T., Serrano-Pozo, A., 2021. Association of APOE Genotype With Heterogeneity of Cognitive Decline Rate in Alzheimer Disease. Neurology 96 (19), e2414–e2428. https://doi.org/10.1212/WNL.0000000000011883.

Reitz, C., Brayne, C., Mayeux, R., 2011. Epidemiology of Alzheimer disease. Nature Reviews. Neurology 7 (3), 137–152. https://doi.org/10.1038/nrneurol.2011.2.

Sando, S.B., Melquist, S., Cannon, A., Hutton, M.L., Sletvold, O., Saltvedt, I., et al., 2008. APOE epsilon 4 lowers age at onset and is a high risk factor for Alzheimer's disease; a case control study from central Norway. BMC Neurology 8, 9. https://doi.org/10.1186/1471-2377-8-9.

Scheltens, P., Blennow, K., Breteler, M.M.B., Strooper, B., de; Frisoni, Giovanni B., Salloway, Stephen; van der Flier, Wiesje Maria, 2016. Alzheimer's disease. the Lancet 388 (10043), 505–517. https://doi.org/10.1016/S0140-6736(15)01124-1.

Schindler, S., Schönknecht, P., Schmidt, L., Anwander, A., Strauß, M., Trampel, R., et al., 2013. Development and evaluation of an algorithm for the computer-assisted segmentation of the human hypothalamus on 7-Tesla magnetic resonance images. PloS One 8 (7), e66394.

Schönknecht, P., Pantel, J., Hartmann, T., Werle, E., Volkmann, M., Essig, M., et al., 2003. Cerebrospinal fluid tau levels in Alzheimer's disease are elevated when compared with vascular dementia but do not correlate with measures of cerebral atrophy. Psychiatry Research 120 (3), 231–238. https://doi.org/10.1016/S0165-1781(03)00197-5.

Senjem, M.L., Gunter, J.L., Shiung, M.M., Petersen, R.C., Jack, C.R., 2005. Comparison of different methodological implementations of voxel-based morphometry in neurodegenerative disease. NeuroImage 26 (2), 600–608. https://doi.org/10.1016/j.neuroimage.2005.02.005.

Shaw, L.M., Vanderstichele, H., Knapik-Czajka, M., Clark, C.M., Aisen, P.S., Petersen, R.C., et al., 2009. Cerebrospinal fluid biomarker signature in Alzheimer's disease neuroimaging initiative subjects. Annals of Neurology 65 (4), 403–413. https://doi.org/10.1002/ana.21610.

Silva, M.V., Ferreira; Loures, Cristina de Mello Gomide; Alves, Luan Carlos Vieira; Souza, Leonardo Cruz de; Borges, Karina Braga Gomes; Carvalho, Maria das Graças, 2019. Alzheimer's disease: risk factors and potentially protective measures. Journal of Biomedical Science 26 (1), 33. https://doi.org/10.1186/s12929-019-0524-y.

Sluimer, J.D., Bouwman, F.H., Vrenken, H., Blankenstein, M.A., Barkhof, F., van der Flier, W.M., Scheltens, P., 2010. Whole-brain atrophy rate and CSF biomarker levels in MCI and AD: a longitudinal study. Neurobiology of Aging 31 (5), 758–764. https://doi.org/10.1016/j.neurobiolaging.2008.06.016.

Spindler, M., Özyurt, J., Thiel, C.M., 2020. Automated diffusion-based parcellation of the hypothalamus reveals subunit-specific associations with obesity. Scientific Reports 10 (1), 22238. https://doi.org/10.1038/s41598-020-79289-9.

Standaert, D.G., Lee, V.M., Greenberg, B.D., Lowery, D.E., Trojanowski, J.Q., 1991. Molecular features of hypothalamic plaques in Alzheimer's disease. The American Journal of Pathology 139 (3), 681–691.

Steward, A., Biel, D., Dewenter, A., Roemer, S., Wagner, F., Dehsarvi, A., et al., 2023. ApoE4 and connectivity-mediated spreading of tau pathology at lower amyloid levels. JAMA Neurology 80 (12), 1295–1306. https://doi.org/10.1001/jamaneurol.2023.4038.

Sullivan, K., 2005. Alternate forms of prose passages for the assessment of auditory-verbal memory. Archives of Clinical Neuropsychology : the Official Journal of the National Academy of Neuropsychologists 20 (6), 745–753. https://doi.org/10.1016/j.acn.2005.04.006.

Suzuki, K., Hirakawa, A., Ihara, R., Iwata, A., Ishii, K., Ikeuchi, T., et al., 2020. Effect of apolipoprotein E ε4 allele on the progression of cognitive decline in the early stage of Alzheimer's disease. Alzheimer's & Dementia (new York N. Y.) 6 (1), e12007. https://doi.org/10.1002/trc2.12007.

Tarawneh, R., Head, D., Allison, S., Buckles, V., Fagan, A.M., Ladenson, J.H., et al., 2015. Cerebrospinal Fluid Markers of Neurodegeneration and Rates of Brain Atrophy in Early Alzheimer Disease. JAMA Neurology 72 (6), 656–665. https://doi.org/10.1001/jamaneurol.2015.0202.

Tezapsidis, N., Johnston, J.M., Smith, M.A., Ashford, J., Wesson; Casadesus, Gemma; Robakis, Nikolaos K., et al., 2009. Leptin: a novel therapeutic strategy for Alzheimer's disease. Journal of Alzheimer's Disease : JAD 16 (4), 731–740. https://doi.org/10.3233/JAD-2009-1021.

Thomas, K., Beyer, F., Lewe, G., Zhang, R., Schindler, S., Schönknecht, P., et al., 2019. Higher body mass index is linked to altered hypothalamic microstructure. Scientific Reports 9 (1). https://doi.org/10.1038/s41598-019-53578-4.

Ulrich-Lai, Y.M., Herman, J.P., 2009. Neural regulation of endocrine and autonomic stress responses. Nature Reviews. Neuroscience 10 (6), 397–409. https://doi.org/10.1038/nrn2647.

Vogel, J.W., Iturria-Medina, Y., Strandberg, O.T., Smith, R., Levitis, E., Evans, A.C., Hansson, O., 2020. Spread of pathological tau proteins through communicating neurons in human Alzheimer's disease. Nature Communications 11 (1), 2612. https://doi.org/10.1038/s41467-020-15701-2.

Walker, L.C., 2018. Prion-like mechanisms in Alzheimer disease. Handbook of Clinical Neurology 153, 303–319. https://doi.org/10.1016/B978-0-444-63945-5.00016-7.

Whitwell, J.L., Jack, C.R., Przybelski, S.A., Parisi, J.E., Senjem, M.L., Boeve, B.F., et al., 2011. Temporoparietal atrophy: a marker of AD pathology independent of clinical

diagnosis. Neurobiology of Aging 32 (9), 1531–1541. https://doi.org/10.1016/j.neurobiolaging.2009.10.012.

Wolff, J., Schindler, S., Lucas, C., Binninger, A.-S., Weinrich, L., Schreiber, J., et al., 2018. A semi-automated algorithm for hypothalamus volumetry in 3 Tesla magnetic resonance images. Psychiatry Research. Neuroimaging 277, 45–51. https://doi.org/10.1016/j.pscychresns.2018.04.007.

Wonderlick, J.S., Ziegler, D.A., Hosseini-Varnamkhasti, P., Locascio, J.J., Bakkour, A., van der Kouwe, A., et al., 2009. Reliability of MRI-derived cortical and subcortical morphometric measures: effects of pulse sequence, voxel geometry, and parallel imaging. NeuroImage 44 (4), 1324–1333. https://doi.org/10.1016/j.neuroimage.2008.10.037.

Wyman, B.T., Harvey, D.J., Crawford, K., Bernstein, M.A., Carmichael, O., Cole, P.E., et al., 2013. Standardization of analysis sets for reporting results from ADNI MRI data. Alzheimer's & Dementia : the Journal of the Alzheimer's Association 9 (3), 332–337. https://doi.org/10.1016/j.jalz.2012.06.004.

Xu, L., Groth, K.M., Pearlson, G., Schretlen, D.J., Calhoun, V.D., 2009. Source-based morphometry: the use of independent component analysis to identify gray matter differences with application to schizophrenia. Human Brain Mapping 30 (3), 711–724. https://doi.org/10.1002/hbm.20540.

Yao, Y., Ying, Y., Deng, Q., Zhang, W., Zhu, H., Lin, Z., et al., 2020. Non-invasive 40-Hz Light Flicker Ameliorates Alzheimer's-Associated Rhythm Disorder via Regulating Central Circadian Clock in Mice. Frontiers in Physiology 11, 294. https://doi.org/10.3389/fphys.2020.00294.

Zhou, X., Wu, R., Zeng, Y., Qi, Z., Ferraro, S., Xu, L., et al., 2022. Choice of Voxel-based Morphometry processing pipeline drives variability in the location of neuroanatomical brain markers. Communications Biology 5 (1), 913. https://doi.org/10.1038/s42003-022-03880-1.